

Article

Wave Dispersion in Multilayered Reinforced Nonlocal Plates under Nonlinearly Varying Initial Stress

Mohammad Reza Farajpour¹, Ali Reza Shahidi² and Ali Farajpour^{2,*}

¹ School of Mechanical Engineering, Borjavarani Center of Applied Science and Technology, Velenjak Campus, University of Applied Science and Technology, Tehran 1594835111, Iran; a.farajpour@ut.ac.ir

² Department of Mechanical Engineering, Isfahan University of Technology, Isfahan 8415683111, Iran; shahidi@cc.iut.ac.ir

* Correspondence: a.farajpouderji@me.iut.ac.ir

Received: 9 July 2020; Accepted: 16 September 2020; Published: 21 September 2020



Abstract: This paper deals with the effects of initial stress on wave propagations in small-scale plates with shape memory alloy (SMA) nanoscale wires. The initial stress is exerted on the small-scale plate along both in-plane directions. A scale-dependent model of plates is developed for taking into consideration size influences on the wave propagation. In addition, in order to take into account the effects of SMA nanoscale wires, the one-dimensional Brinson's model is applied. A set of coupled differential equations is obtained for the non-uniformly prestressed small-scale plate with SMA nanoscale wires. An exact solution is obtained for the phase and group velocities of the prestressed small-scale system. The influences of non-uniformly distributed initial stresses as well as scale and SMA effects on the phase and group velocities are explored and discussed. It is found that initial stresses as well as the orientation and volume fraction of SMA nanoscale wires can be used as a controlling factor for the wave propagation characteristics of small-scale plates.

Keywords: wave propagation; shape memory alloy; nanoscale wires; prestressed plates

1. Introduction

Nanomaterials have attracted noticeable interest in different engineering-related disciplines since last decade due to their promising thermo-electro-mechanical properties [1–4]. Initial stresses influence the energy efficiency and performance of many macroscale and small-scale electromechanical devices and machines since the mechanical response of the fundamental parts of these systems is changed in the presence of initial stresses [5,6]. Many factors such as imprecision in manufacturing processes and inappropriate operating conditions can cause initial stresses. In many real situations, completely eliminating initial stresses is difficult and costly. Therefore, to have better energy efficiency and performance, it is important to increase our level of knowledge of the influences of initial stresses on the mechanical response [7].

A notable amount of effort has been made in recent years in order to analyze the influences of initial stresses on the mechanical response of small-scale structures using elasticity models [8]. Since the mechanical response is highly scale-dependent at ultrasmall levels [9–17], modified elasticity theories incorporating size effects are often used for small-scale structures [18–24]. Wang and Cai [25] investigated the influences of initial stresses on the vibrational characteristics of multi-walled carbon nanotubes (CNTs) via a elasticity model. Furthermore, Song et al. [26] examined the initial stress effects on the wave propagation in CNTs via applying a nonlocal model of elasticity. Heireche et al. [27] also explored sound wave propagations in a single-walled CNT subject to initial longitudinal stresses. In another investigation, Güven [28] studied the effects of initial stresses on the vibrational characteristics

of CNTs under a magnetic field. In addition, in a continuum-based study conducted by Selim et al. [29], a theoretical model was developed for analyzing initial stress effects on the wave propagation characteristics of CNTs. Shen et al. [30] developed a scale-dependent elasticity model for the vibration of nanoscale mechanical sensors using double-walled CNTs under initial longitudinal stresses.

Besides developing elasticity models for small-scale tubes such as CNTs under initial stresses, the mechanical response of small-scale plates with initial stresses has been analyzed via scale-dependent models. Asemi et al. [31] examined initial stress effects on the vibrational characteristics of a system of two piezoelectric nanoscale plates employing a nonlocal model of plates. In another study, size effects together with the influences of initial stresses on the flexural wave propagations in nanoscale plates [32] were explored using the nonlocal elasticity. Moreover, the effects of uniaxial initial stress on the nonlocal vibrational response of nanoplates was examined in the literature [33]. Karami et al. [34] also analyzed initial stress effects on the wave dispersion of graphene sheets mounted on an elastic matrix. Ebrahimi and Shafiei [35] developed a modified plate model for the vibrational response of graphene sheets with initial stresses employing Reddy’s higher-order theory of shear deformations. In another investigation by Mohammadi et al. [36], the influences of shear initial stresses on the vibration of small-scale plates embedded in an elastic matrix were explored.

Composite ultrasmall structures such as hybrid plates have been synthesized and applied in a variety of applications in recent years [2,3,37]. On the other hand, due to the excellent mechanical properties of shape memory alloy (SMA) wires, they have been used for many different applications ranging from reinforced smart concrete [38] to robotic neurosurgery [39]. Furthermore, different applications of SMA small-scale structures in micro/nanoscale electromechanical systems have recently been reported [40]. In this article, the influences of nonlinearly varying initial stress on the wave propagation in multilayered small-scale plates with SMA nanoscale wires are investigated. The mechanism of wave dispersion in typical small-scale plates is known to researchers. However, to the best of our knowledge, no study has been reported on wave dispersion in reinforced nonlocal plates under nonlinear initial stresses. For this study, a scale-dependent model of plates is proposed employing the nonlocal elasticity. The effects of SMA nanoscale wires on the wave propagation are modeled using Brinson’s model. The coupled differential equations for scale-dependent wave propagations in the small-scale plate are presented. The phase and group velocities of the small-scale system are obtained. The effects of non-uniformly distributed initial stresses in conjunction with size and SMA effects on the phase and group velocities are examined. The theoretical formulation and accurate analysis performed in this article would be useful in the design and manufacture of cutting-edge technology-based machines in the field, especially in developing devices and tools for analyzing wave dispersion and stress evaluation in ultrasmall structures.

2. Prestressed Small-Scale Plates with SMA Nanoscale Wires

In this section, wave propagations in prestressed small-scale plates with SMA nanoscale wires are formulated using a scale-dependent plate model. Figure 1 illustrates a small-scale plate made of five layers reinforced by SMA nanoscale wires. Let us indicate the length, thickness and width of each layer by l_x , h and l_y , respectively. Furthermore, Poisson’s ratio, elasticity moduli, shear modulus and density of the small-scale plate are denoted by ν_{12}^{LP} , E_i^{LP} , G_{12}^{LP} and ρ_{LP} , respectively. For these properties, we have [41]

$$\begin{aligned}
 E_1^{LP}(\zeta) &= E_W \left[V_W^{SMA}(\zeta) \right] + E_P \left[1 - V_W^{SMA}(\zeta) \right], \\
 \rho_{LP}(\zeta) &= \rho_W \left[V_W^{SMA}(\zeta) \right] + \rho_P \left[1 - V_W^{SMA}(\zeta) \right], \\
 \nu_{12}^{LP}(\zeta) &= \nu_W \left[V_W^{SMA}(\zeta) \right] + \nu_P \left[1 - V_W^{SMA}(\zeta) \right], \\
 E_2^{LP}(\zeta) &= \frac{E_W E_P}{\left\{ E_P \left[V_W^{SMA}(\zeta) \right] + E_W \left[1 - V_W^{SMA}(\zeta) \right] \right\}'}, \\
 G_{12}^{LP}(\zeta) &= \frac{G_W G_P}{\left\{ G_P \left[V_W^{SMA}(\zeta) \right] + G_W \left[1 - V_W^{SMA}(\zeta) \right] \right\}'},
 \end{aligned} \tag{1}$$

where ζ and V_W^{SMA} indicate the martensite fraction and volume fraction of SMA nanoscale wires, respectively; “LP”, “W” and “P” are used to refer to the laminated plate, SMA nanoscale wires and plate, respectively. Using one-dimensional Brinson’s model, for a SMA nanoscale wire, one obtains [42,43]

$$E_W(\zeta) = \frac{E_{mar}E_{aus}}{E_{mar}(1 - \zeta) + E_{aus}\zeta}, \tag{2}$$

in which “mar” and “aus” are used to refer to the martensite and austenite phases, respectively. The martensite fraction is determined by two dominant factors as follows

$$\zeta = \zeta_{tem} + \zeta_{str}. \tag{3}$$

where

$$\begin{Bmatrix} \zeta_{str} \\ \zeta_{tem} \end{Bmatrix} = \begin{Bmatrix} \zeta_{str0} \\ \zeta_{tem0} \end{Bmatrix} - \left(\frac{\zeta_0 - \zeta}{\zeta_0} \right) \begin{Bmatrix} \zeta_{str0} \\ \zeta_{tem0} \end{Bmatrix}. \tag{4}$$

Here “str”, “tem” and “0” denote the stress, temperature and initial value of a factor, respectively. Using one-dimensional Brinson’s model, we have the following relation for the martensite fraction

$$\zeta = \frac{\zeta_0}{2} \cos[\lambda_c(C_A T - C_A A_{sta} - \sigma)] + \frac{\zeta_0}{2} \tag{5}$$

for $C_A T - C_A A_{fin} < \sigma < C_A T - C_A A_{sta}$ and $T > A_{sta}$,

where

$$\lambda_c = \frac{\pi}{C_A(A_{fin} - A_{sta})}, \tag{6}$$

where T and σ are, respectively, the temperature and stress; A_{fin} , A_{sta} and C_A are, respectively, the finish temperature of the austenite phase, start temperature of this phase and critical stress slope. Let us denote the mid-plane displacement in z , y and x directions by w , v and u , respectively. For the normal and shear strains, one can write

$$\begin{aligned} \varepsilon_{xx} &= \varepsilon_{xx}^0 - z\kappa_{xx}, \\ \varepsilon_{yy} &= \varepsilon_{yy}^0 - z\kappa_{yy}, \\ \gamma_{xy} &= \gamma_{xy}^0 - z\kappa_{xy}, \end{aligned} \tag{7}$$

where

$$\begin{Bmatrix} \varepsilon_{xx}^0 \\ \varepsilon_{yy}^0 \\ \gamma_{xy}^0 \end{Bmatrix} = \begin{Bmatrix} \frac{\partial u}{\partial x} \\ \frac{\partial v}{\partial y} \\ \frac{\partial v}{\partial x} + \frac{\partial u}{\partial y} \end{Bmatrix}, \begin{Bmatrix} \kappa_{xx} \\ \kappa_{yy} \\ \kappa_{xy} \end{Bmatrix} = \begin{Bmatrix} \frac{\partial^2 w}{\partial x^2} \\ \frac{\partial^2 w}{\partial y^2} \\ 2 \frac{\partial^2 w}{\partial y \partial x} \end{Bmatrix}. \tag{8}$$

Taking into account a scale parameter in the form of $\mu_{nl} = (e_0 a_c)^2$ in which e_0 and a_c are a calibration constant and an internal characteristic length [44,45], the constitutive relation is

$$\begin{aligned} \begin{Bmatrix} \sigma_{xx}^{(k)} \\ \sigma_{yy}^{(k)} \\ \sigma_{xy}^{(k)} \end{Bmatrix} - \mu_{nl} \nabla^2 \begin{Bmatrix} \sigma_{xx}^{(k)} \\ \sigma_{yy}^{(k)} \\ \sigma_{xy}^{(k)} \end{Bmatrix} &= \left[\tilde{\mathbf{C}}^{(k)}(\zeta, \phi_k) \right] \begin{Bmatrix} \varepsilon_{xx}^0 \\ \varepsilon_{yy}^0 \\ \gamma_{xy}^0 \end{Bmatrix} \\ -z \left[\tilde{\mathbf{C}}^{(k)}(\zeta, \phi_k) \right] \begin{Bmatrix} \kappa_{xx} \\ \kappa_{yy} \\ \kappa_{xy} \end{Bmatrix} &+ V_{W,k}^{SMA} \sigma_{RS}^{(k)} \begin{Bmatrix} \eta_1(\phi_k) \\ \eta_2(\phi_k) \\ \eta_3(\phi_k) \end{Bmatrix}, \end{aligned} \tag{9}$$

where

$$\begin{aligned} \left[\tilde{\mathbf{C}}^{(k)}(\zeta, \phi_k) \right] &= \begin{bmatrix} \tilde{C}_{11}^{(k)}(\zeta, \phi_k) & \tilde{C}_{12}^{(k)}(\zeta, \phi_k) & \tilde{C}_{16}^{(k)}(\zeta, \phi_k) \\ \tilde{C}_{12}^{(k)}(\zeta, \phi_k) & \tilde{C}_{22}^{(k)}(\zeta, \phi_k) & \tilde{C}_{26}^{(k)}(\zeta, \phi_k) \\ \tilde{C}_{16}^{(k)}(\zeta, \phi_k) & \tilde{C}_{26}^{(k)}(\zeta, \phi_k) & \tilde{C}_{66}^{(k)}(\zeta, \phi_k) \end{bmatrix}, \\ \begin{Bmatrix} \eta_1(\phi_k) \\ \eta_2(\phi_k) \\ \eta_3(\phi_k) \end{Bmatrix} &= \begin{Bmatrix} \cos^2(\phi_k) \\ \sin^2(\phi_k) \\ \cos(\phi_k) \sin(\phi_k) \end{Bmatrix}. \end{aligned} \tag{10}$$

In Equations (9) and (10), $\tilde{C}_{ij}^{(k)}$, $\sigma_{RS}^{(k)}$ and ϕ_k stand for the elasticity constants of the plate, the recovery stress and angle of SMA nanoscale wires, respectively; ∇^2 represents the Laplace operator. Taking into account a reinforced small-scale plate made of n layers, the stress resultants are

$$\begin{aligned} N_{xx} &= \sum_{l=1}^n \int_{z_{l-1}}^{z_l} \sigma_{xx}^{(l)} dz, \quad N_{yy} = \sum_{l=1}^n \int_{z_{l-1}}^{z_l} \sigma_{yy}^{(l)} dz, \\ N_{xy} &= \sum_{l=1}^n \int_{z_{l-1}}^{z_l} \sigma_{xy}^{(l)} dz, \quad M_{xx} = \sum_{l=1}^n \int_{z_{l-1}}^{z_l} \sigma_{xx}^{(l)} z dz, \\ M_{yy} &= \sum_{l=1}^n \int_{z_{l-1}}^{z_l} \sigma_{yy}^{(l)} z dz, \quad M_{xy} = \sum_{l=1}^n \int_{z_{l-1}}^{z_l} \sigma_{xy}^{(l)} z dz. \end{aligned} \tag{11}$$

Furthermore, the recovery stress resultants are as follows

$$\begin{aligned} N_{xx}^{RS} &= \sum_{l=1}^n \int_{z_{l-1}}^{z_l} V_{W,l}^{SMA} \sigma_{RS}^{(l)} \eta_1(\phi_l) dz, \\ N_{yy}^{RS} &= \sum_{l=1}^n \int_{z_{l-1}}^{z_l} V_{W,l}^{SMA} \sigma_{RS}^{(l)} \eta_2(\phi_l) dz, \\ N_{xy}^{RS} &= \sum_{l=1}^n \int_{z_{l-1}}^{z_l} V_{W,l}^{SMA} \sigma_{RS}^{(l)} \eta_3(\phi_l) dz, \\ M_{xx}^{RS} &= \sum_{l=1}^n \int_{z_{l-1}}^{z_l} V_{W,l}^{SMA} \sigma_{RS}^{(l)} \eta_1(\phi_l) z dz, \\ M_{yy}^{RS} &= \sum_{l=1}^n \int_{z_{l-1}}^{z_l} V_{W,l}^{SMA} \sigma_{RS}^{(l)} \eta_2(\phi_l) z dz, \\ M_{xy}^{RS} &= \sum_{l=1}^n \int_{z_{l-1}}^{z_l} V_{W,l}^{SMA} \sigma_{RS}^{(l)} \eta_3(\phi_l) z dz. \end{aligned} \tag{12}$$

Employing Equations (9) and (11) together with Equation (8), we obtain the following equations for the stress resultants

$$\begin{Bmatrix} N_{xx} \\ N_{yy} \\ N_{xy} \end{Bmatrix} - \mu_{nl} \nabla^2 \begin{Bmatrix} N_{xx} \\ N_{yy} \\ N_{xy} \end{Bmatrix} = [\tilde{\mathbf{K}}] \begin{Bmatrix} \frac{\partial u}{\partial x} \\ \frac{\partial v}{\partial y} \\ \frac{\partial v}{\partial x} + \frac{\partial u}{\partial y} \end{Bmatrix} - [\tilde{\mathbf{Q}}] \begin{Bmatrix} \frac{\partial^2 w}{\partial x^2} \\ \frac{\partial^2 w}{\partial y^2} \\ 2 \frac{\partial^2 w}{\partial y \partial x} \end{Bmatrix} + \begin{Bmatrix} N_{xx}^{RS} \\ N_{yy}^{RS} \\ N_{xy}^{RS} \end{Bmatrix}, \tag{13}$$

$$\begin{Bmatrix} M_{xx} \\ M_{yy} \\ M_{xy} \end{Bmatrix} - \mu_{nl} \nabla^2 \begin{Bmatrix} M_{xx} \\ M_{yy} \\ M_{xy} \end{Bmatrix} = [\tilde{\mathbf{Q}}] \begin{Bmatrix} \frac{\partial u}{\partial x} \\ \frac{\partial v}{\partial y} \\ \frac{\partial v}{\partial x} + \frac{\partial u}{\partial y} \end{Bmatrix} - [\tilde{\mathbf{S}}] \begin{Bmatrix} \frac{\partial^2 w}{\partial x^2} \\ \frac{\partial^2 w}{\partial y^2} \\ 2 \frac{\partial^2 w}{\partial y \partial x} \end{Bmatrix} + \begin{Bmatrix} M_{xx}^{RS} \\ M_{yy}^{RS} \\ M_{xy}^{RS} \end{Bmatrix}, \tag{14}$$

where

$$[\tilde{\mathbf{K}}] = \begin{bmatrix} \tilde{K}_{11} & \tilde{K}_{12} & \tilde{K}_{16} \\ \tilde{K}_{12} & \tilde{K}_{22} & \tilde{K}_{26} \\ \tilde{K}_{16} & \tilde{K}_{26} & \tilde{K}_{66} \end{bmatrix}, \quad [\tilde{\mathbf{Q}}] = \begin{bmatrix} \tilde{Q}_{11} & \tilde{Q}_{12} & \tilde{Q}_{16} \\ \tilde{Q}_{12} & \tilde{Q}_{22} & \tilde{Q}_{26} \\ \tilde{Q}_{16} & \tilde{Q}_{26} & \tilde{Q}_{66} \end{bmatrix}, \quad [\tilde{\mathbf{S}}] = \begin{bmatrix} \tilde{S}_{11} & \tilde{S}_{12} & \tilde{S}_{16} \\ \tilde{S}_{12} & \tilde{S}_{22} & \tilde{S}_{26} \\ \tilde{S}_{16} & \tilde{S}_{26} & \tilde{S}_{66} \end{bmatrix}, \tag{15}$$

and

$$\begin{pmatrix} \bar{K}_{ij} \\ \bar{Q}_{ij} \\ \bar{S}_{ij} \end{pmatrix} = \begin{pmatrix} \sum_{l=1}^n \bar{C}_{ij}^{(l)} (z_l - z_{l-1}) \\ \sum_{l=1}^n \frac{\bar{C}_{ij}^{(l)}}{2} (z_l^2 - z_{l-1}^2) \\ \sum_{l=1}^n \frac{\bar{C}_{ij}^{(l)}}{3} (z_l^3 - z_{l-1}^3) \end{pmatrix}. \tag{16}$$

Applying Hamilton’s principle leads to motion equations as follows

$$\frac{\partial N_{xx}}{\partial x} + \frac{\partial N_{xy}}{\partial y} = m_{LP} \frac{\partial^2 u}{\partial t^2}, \tag{17}$$

$$\frac{\partial N_{xy}}{\partial x} + \frac{\partial N_{yy}}{\partial y} = m_{LP} \frac{\partial^2 v}{\partial t^2}, \tag{18}$$

$$\begin{aligned} \frac{\partial^2 M_{yy}}{\partial y^2} + 2 \frac{\partial^2 M_{xy}}{\partial x \partial y} + \frac{\partial^2 M_{xx}}{\partial x^2} + \frac{\partial}{\partial y} \left(N_{xy} \frac{\partial w}{\partial x} + N_{yy} \frac{\partial w}{\partial y} \right) \\ + \frac{\partial}{\partial x} \left(N_{xx} \frac{\partial w}{\partial x} + N_{xy} \frac{\partial w}{\partial y} \right) = m_{LP} \frac{\partial^2 w}{\partial t^2}, \end{aligned} \tag{19}$$

where m_{LP} is the mass per unit area of the small-scale plate. Substituting Equations (13) and (14) into Equations (17)–(19), the coupled equations for the wave propagation in the small-scale plate are obtained as

$$\begin{aligned} \bar{K}_{66} \frac{\partial^2 u}{\partial y^2} + \bar{K}_{11} \frac{\partial^2 u}{\partial x^2} + 2\bar{K}_{16} \frac{\partial^2 u}{\partial y \partial x} + \bar{K}_{26} \frac{\partial^2 v}{\partial y^2} + \bar{K}_{16} \frac{\partial^2 v}{\partial x^2} \\ + (\bar{K}_{66} + \bar{K}_{12}) \frac{\partial^2 v}{\partial y \partial x} - \left[\bar{Q}_{26} \frac{\partial^3 w}{\partial y^3} + (\bar{Q}_{12} + 2\bar{Q}_{66}) \frac{\partial^3 w}{\partial y^2 \partial x} \right. \\ \left. + 3\bar{Q}_{16} \frac{\partial^3 w}{\partial y \partial x^2} + \bar{Q}_{11} \frac{\partial^3 w}{\partial x^3} \right] = m_{LP} \frac{\partial^2 u}{\partial t^2} - m_{LP} \mu_{nl} \nabla^2 \frac{\partial^2 u}{\partial t^2}, \end{aligned} \tag{20}$$

$$\begin{aligned} \bar{K}_{26} \frac{\partial^2 u}{\partial y^2} + \bar{K}_{16} \frac{\partial^2 u}{\partial x^2} + (\bar{K}_{66} + \bar{K}_{12}) \frac{\partial^2 u}{\partial y \partial x} + \bar{K}_{22} \frac{\partial^2 v}{\partial y^2} \\ + \bar{K}_{66} \frac{\partial^2 v}{\partial x^2} + 2\bar{K}_{26} \frac{\partial^2 v}{\partial y \partial x} - \left[\bar{Q}_{22} \frac{\partial^3 w}{\partial y^3} + 3\bar{Q}_{26} \frac{\partial^3 w}{\partial y^2 \partial x} \right. \\ \left. + (\bar{Q}_{12} + 2\bar{Q}_{66}) \frac{\partial^3 w}{\partial y \partial x^2} + \bar{Q}_{16} \frac{\partial^3 w}{\partial x^3} \right] = m_{LP} \frac{\partial^2 v}{\partial t^2} - m_{LP} \mu_{nl} \nabla^2 \frac{\partial^2 v}{\partial t^2}, \end{aligned} \tag{21}$$

$$\begin{aligned} \bar{Q}_{26} \frac{\partial^3 u}{\partial y^3} + 3\bar{Q}_{16} \frac{\partial^3 u}{\partial y \partial x^2} + (\bar{Q}_{12} + 2\bar{Q}_{66}) \frac{\partial^3 u}{\partial y^2 \partial x} + \bar{Q}_{11} \frac{\partial^3 u}{\partial x^3} \\ + \bar{Q}_{22} \frac{\partial^3 v}{\partial y^3} + (\bar{Q}_{12} + 2\bar{Q}_{66}) \frac{\partial^3 v}{\partial y \partial x^2} + 3\bar{Q}_{26} \frac{\partial^3 v}{\partial y^2 \partial x} + \bar{Q}_{16} \frac{\partial^3 v}{\partial x^3} \\ - \left[\bar{S}_{22} \frac{\partial^4 w}{\partial y^4} + 2(\bar{S}_{12} + 2\bar{S}_{66}) \frac{\partial^4 w}{\partial y^2 \partial x^2} + 4\bar{S}_{26} \frac{\partial^4 w}{\partial y^3 \partial x} + \bar{S}_{11} \frac{\partial^4 w}{\partial x^4} \right. \\ \left. + 4\bar{S}_{16} \frac{\partial^4 w}{\partial x^3 \partial y} \right] + (N_{yy}^{RS} + N_{yy}^{PS}) \frac{\partial^2 w}{\partial y^2} + (N_{xx}^{RS} + N_{xx}^{PS}) \frac{\partial^2 w}{\partial x^2} + 2N_{xy}^{RS} \frac{\partial^2 w}{\partial x \partial y} \\ - \mu_{nl} \left[(N_{yy}^{RS} + N_{yy}^{PS}) \frac{\partial^4 w}{\partial y^4} + (N_{xx}^{RS} + N_{xx}^{PS}) \frac{\partial^4 w}{\partial x^4} + 2N_{xy}^{RS} \frac{\partial^4 w}{\partial x^3 \partial y} \right. \\ \left. + 2N_{xy}^{RS} \frac{\partial^4 w}{\partial x \partial y^3} + (N_{xx}^{RS} + N_{yy}^{RS} + N_{xx}^{PS} + N_{yy}^{PS}) \frac{\partial^4 w}{\partial y^2 \partial x^2} \right] \\ = m_{LP} \frac{\partial^2 w}{\partial t^2} - m_{LP} \mu_{nl} \nabla^2 \frac{\partial^2 w}{\partial t^2}, \end{aligned} \tag{22}$$

where N_{ij}^{PS} is the in-plane load induced by initial stresses, which is obtained by

$$N_{xx}^{PS} = \sum_{l=1}^n \int_{z_{l-1}}^{z_l} \sigma_{xx}^{PS(l)} dz, \quad N_{yy}^{PS} = \sum_{l=1}^n \int_{z_{l-1}}^{z_l} \sigma_{yy}^{PS(l)} dz, \tag{23}$$

where $\sigma_{ij(l)}^{PS}$ denotes initial stresses. Assuming non-uniformly distributed initial stresses along the thickness of the small-scale plate, we have

$$\begin{aligned} \bar{\sigma}_{xx(k)}^{PS} &= a\bar{\sigma}_{xx(1)}^{PS} (\bar{z}_k - \bar{z}_1)^b + \bar{\sigma}_{xx(1)}^{PS}, \\ \bar{\sigma}_{yy(k)}^{PS} &= a\bar{\sigma}_{yy(1)}^{PS} (\bar{z}_k - \bar{z}_1)^b + \bar{\sigma}_{yy(1)}^{PS}, \end{aligned} \tag{24}$$

in which $\bar{z}_j = z_j/h$ and $\bar{\sigma}_{ij(k)}^{PS} = \sigma_{ij(k)}^{PS} / C_{11}^{(k)}$. Moreover, a and b are constants, which determine the variation of initial stress. In order to determine the phase and group velocities of the small-scale plate with SMA nanoscale wires, the displacements along the length, width and thickness directions are expressed as [46]

$$\begin{aligned} u(x, y, t) &= \hat{U} \exp(-i\omega t + ik_x x + ik_y y), \\ v(x, y, t) &= \hat{V} \exp(-i\omega t + ik_x x + ik_y y), \\ w(x, y, t) &= \hat{W} \exp(-i\omega t + ik_x x + ik_y y), \end{aligned} \tag{25}$$

in which k_j ($j = x, y$) represents wave numbers; \hat{U} , \hat{V} and \hat{W} indicate wave amplitude coefficients; ω is the frequency of the small-scale plate. Substituting Equation (25) into Equations (20)–(22) leads to a matrix equation as follows

$$[\tilde{\Pi}] \left\{ \hat{\Delta} \right\} - \omega^2 [\tilde{\Lambda}] \left\{ \hat{\Delta} \right\} = 0, \tag{26}$$

where

$$[\tilde{\Pi}] = \begin{bmatrix} \tilde{\Pi}_{11} & \tilde{\Pi}_{12} & \tilde{\Pi}_{13} \\ \tilde{\Pi}_{21} & \tilde{\Pi}_{22} & \tilde{\Pi}_{23} \\ \tilde{\Pi}_{31} & \tilde{\Pi}_{32} & \tilde{\Pi}_{33} \end{bmatrix}, [\tilde{\Lambda}] = \begin{bmatrix} \tilde{\Lambda}_{11} & \tilde{\Lambda}_{12} & \tilde{\Lambda}_{13} \\ \tilde{\Lambda}_{21} & \tilde{\Lambda}_{22} & \tilde{\Lambda}_{23} \\ \tilde{\Lambda}_{31} & \tilde{\Lambda}_{32} & \tilde{\Lambda}_{33} \end{bmatrix}, \left\{ \hat{\Delta} \right\} = \begin{Bmatrix} \hat{U} \\ \hat{V} \\ \hat{W} \end{Bmatrix}. \tag{27}$$

The frequency of the small-scale plate with SMA nanoscale wires is calculated from the following relation

$$\left| [\tilde{\Pi}] - \omega^2 [\tilde{\Lambda}] \right| = 0, \tag{28}$$

where “|” is used to denote the determinant. Assuming $k = k_x = k_y$, the general wave number is obtained as $K = \sqrt{k_x^2 + k_y^2} = \sqrt{2}k$. The phase velocity (c_p) is defined as

$$c_p = \frac{\omega}{K}. \tag{29}$$

In addition, the group velocity (c_g) is determined as follows

$$c_g = \frac{d\omega}{dK}. \tag{30}$$

An ultrasonic wave dispersion in a reinforced multilayered small-scale plate depends on the stress, any components and their distributions, as well as the drive frequency. It is important to notice that there are many studies on stress evaluation by the ultrasonic velocity [47,48]. In other words, a wave propagation analysis can be used as a tool to measure the stress in a structural element.

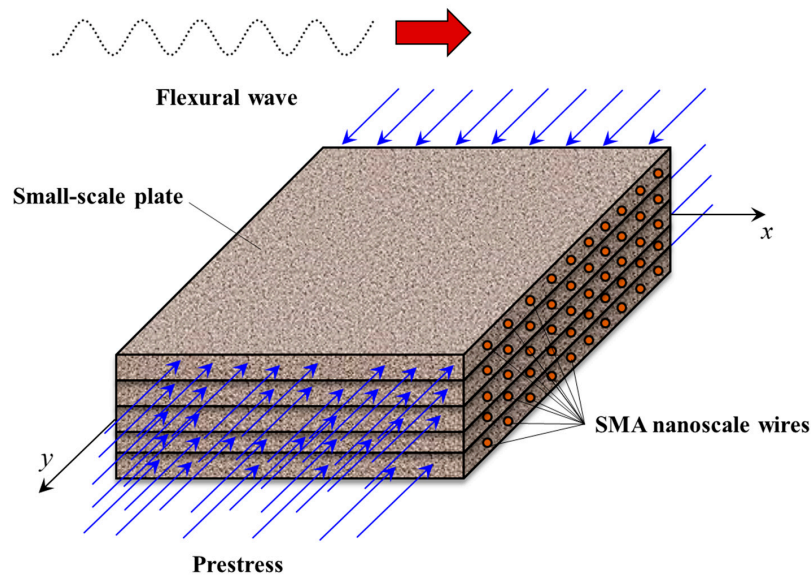


Figure 1. Wave propagation in a prestressed small-scale plate with shape memory alloy (SMA) nanoscale wires.

3. Results and Discussion

Figure 2 compares the calculated group velocities with those determined in the literature for wave propagations in a small-scale plate without SMA nanoscale wires [49]. The nonlocal parameter, thickness, Poisson’s ratio, elasticity modulus and mass per volume of the small-scale plate are set to 1 nm, 0.34 nm, 0.25, 1.06 TPa and 2250 kg/m³, respectively [49]. It is found that the calculated results excellently match those determined in the literature.

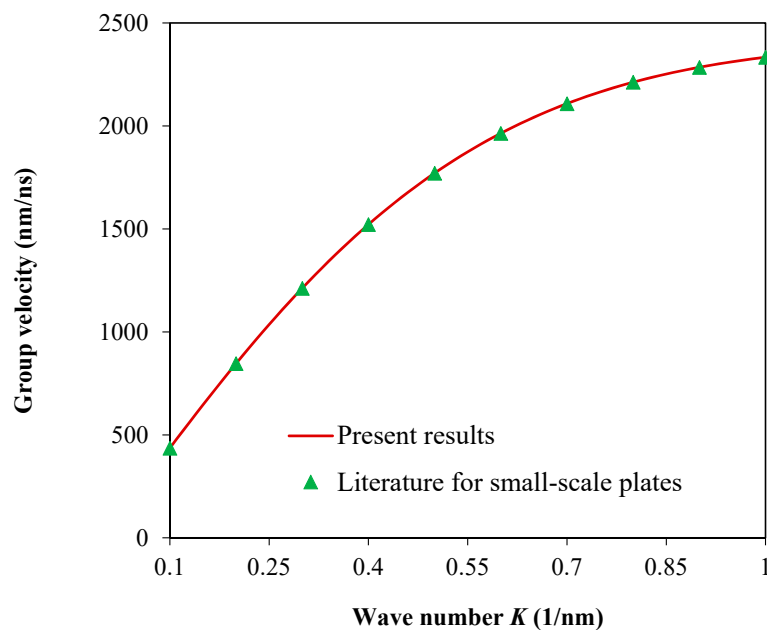


Figure 2. Group velocities calculated by the current modeling and those calculated in Ref. [49] for wave propagations in small-scale plates.

The effects of initial stress ratio together with wave number effects on the phase velocity and group velocity of small-scale plates with SMA nanoscale wires are indicated in Figures 3 and 4, respectively. The initial stress ratio is defined as $\bar{\sigma}_{xx(1)}^{PS} = \sigma_{xx(1)}^{PS} / C_{11}^{(1)}$. A biaxial initial stress condition with a tension ratio of 1:1 is taken into account. It is assumed that all five layers have the same initial stress and

tension ratio. The side length and thickness of each square layer are, respectively, set to 150 and 3 nm. The ratio of the nonlocal parameter to the side length (scale parameter) is 0.02. The physical properties of SMA nanoscale wires are taken as $\nu_W = 0.3$, $\rho_W = 6450 \text{ kg/m}^3$, $E_W = 30 \text{ GPa}$, $\phi_k = 0^0$, $V_W^{SMA} = 0.3$ and $\sigma_{RS} = 0.2 \text{ GPa}$ while for the small-scale plate, we have $\nu_P = 0.3$, $\rho_P = 1600 \text{ kg/m}^3$ and $E_P = 3.44 \text{ GPa}$ [50]. These physical properties are considered for each figure unless otherwise stated. From Figures 3 and 4, it is found that increasing the tensile initial ratio leads to an increase in both phase and group velocities. The reason behind this phenomenon is that as the tensile biaxial initial stress is increased, the stiffness of the small-scale plate improves, and consequently the frequency increases. This leads to a noticeable increase in the phase velocity according to Equation (29).

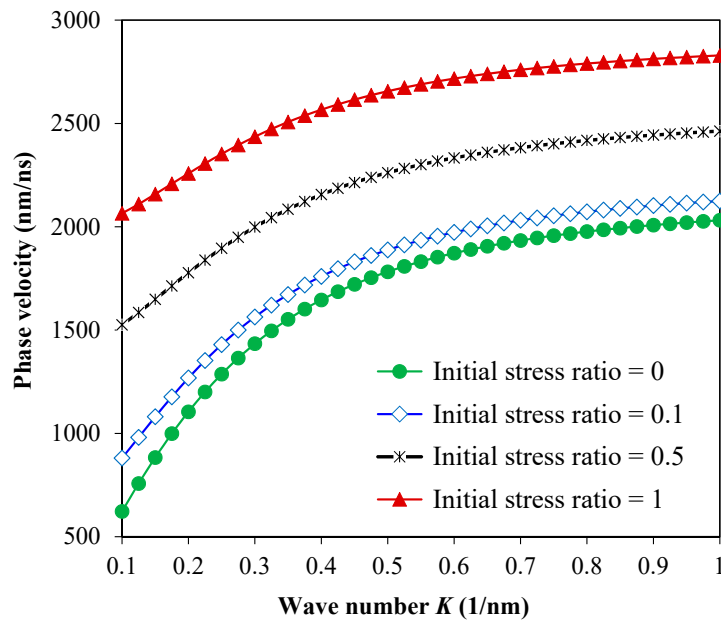


Figure 3. Effects of the initial stress ratio on the phase velocity of small-scale plates with SMA nanoscale wires.

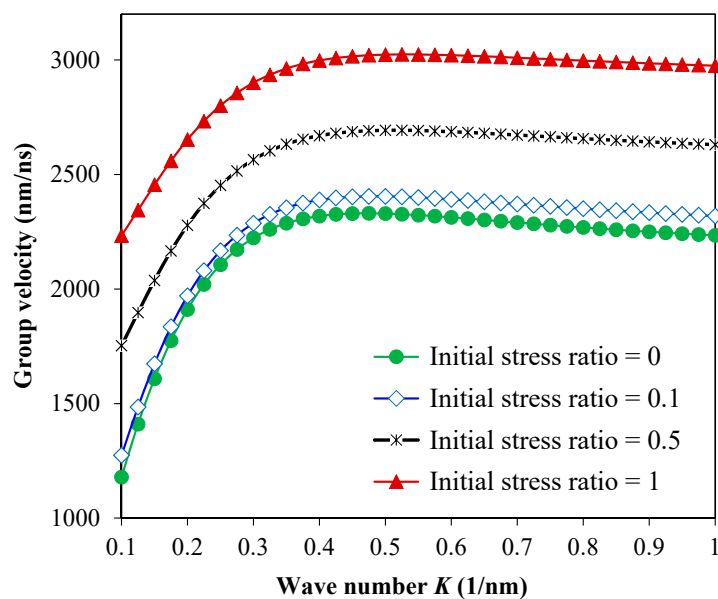


Figure 4. Effects of the initial stress ratio on the group velocity of small-scale plates with SMA nanoscale wires.

Scale effects together with initial stress effects on the phase and group velocities of small-scale plates with SMA nanoscale wires are, respectively, indicated in Figures 5 and 6. The initial stress ratio is set to 0.5 for the cases with initial stress. It is found that greater scale parameters lead to lower phase and group velocities. It is rooted in the fact that greater nonlocal scale parameters reduce the stiffness, and thus are associated with lower frequencies. Therefore, the phase velocity of reinforced multilayered small-scale plates is significantly decreased as the scale parameter of stress nonlocality increases. The effects of the volume fraction of SMA nanoscale wires on the phase and group velocities are also indicated in Figures 7 and 8, respectively. The initial stress ratio and scale parameter are 0.5 and 0.02, respectively. It is concluded that both group and phase velocities are sensitive to the volume fraction. Increasing this parameter slightly increases these velocities. It implies that the volume fraction of SMA nanoscale wires can be utilized as a controlling factor for wave propagation characteristics of small-scale plates.

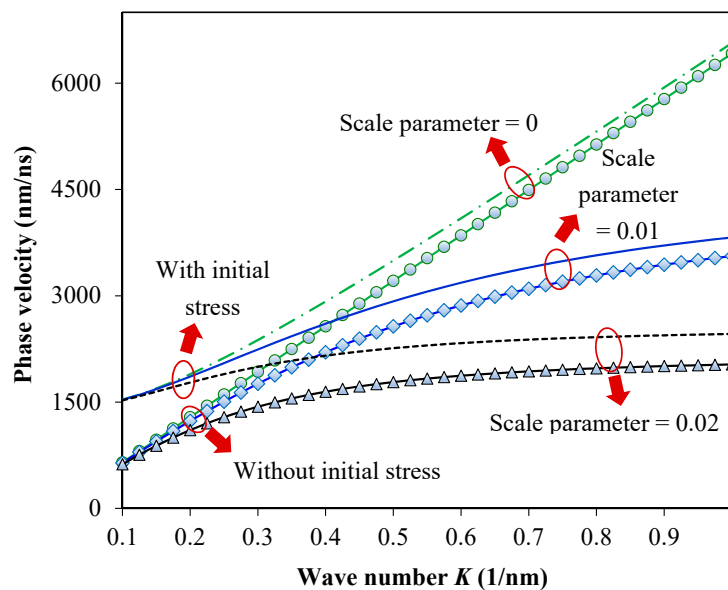


Figure 5. Effects of the scale parameter together with initial stress influences on the phase velocity of small-scale plates with SMA nanoscale wires.

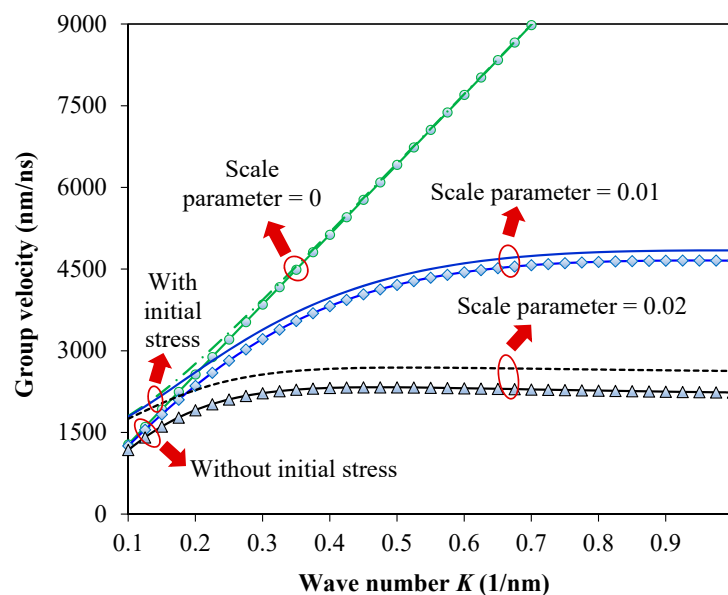


Figure 6. Effects of the scale parameter together with initial stress influences on the group velocity of small-scale plates with SMA nanoscale wires.

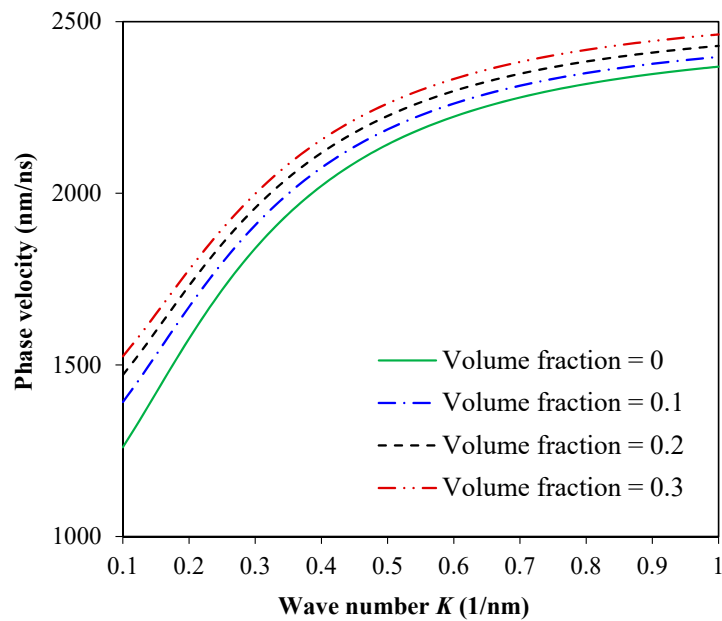


Figure 7. Effects of the volume fraction on the phase velocity of small-scale plates with SMA nanoscale wires.

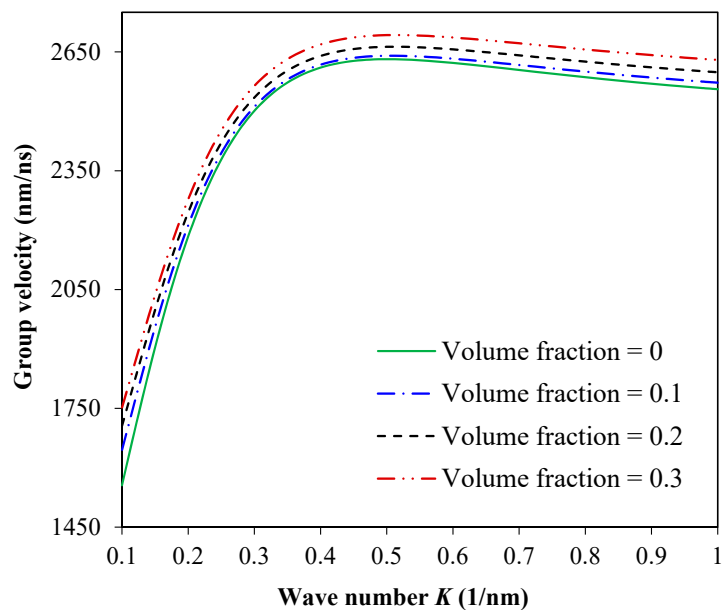


Figure 8. Effects of the volume fraction on the group velocity of small-scale plates with SMA nanoscale wires.

The recovery stress effects in conjunction with the influences of the wave number on the phase and group velocities of small-scale plates with SMA nanoscale wires are, respectively, indicated in Figures 9 and 10. The initial stress ratio, scale parameter and volume fraction are 0.5, 0.02 and 0.3, respectively. Greater recovery stresses increase both phase and group velocities. It implies that the recovery stress can also be used as a controlling factor for phase and group velocities of small-scale plates. In fact, enhanced recovery stresses are linked to a slight increase in the total equivalent structural stiffness of reinforced multilayered nonlocal plates, leading to slightly increased frequencies, and thus a small increase in the phase velocity. In addition, the influences of initial stress and the orientation of SMA nanoscale wires on the phase and group velocities are highlighted in Figures 11 and 12, respectively. The recovery stress and wave number are set to 0.2 GPa and 1.0 1/nm. The maximum phase and group velocities are obtained for $\phi_k = 45^\circ$ for $k = 1, 2, \dots, 5$. Initial stresses are assumed to be tensile

in this case, and thus they act as an improving agent for the total equivalent stiffness of reinforced multilayered nonlocal plates. This initial condition consequently yields enhanced frequencies and improved phase velocities as one can observe from Figures 11 and 12.

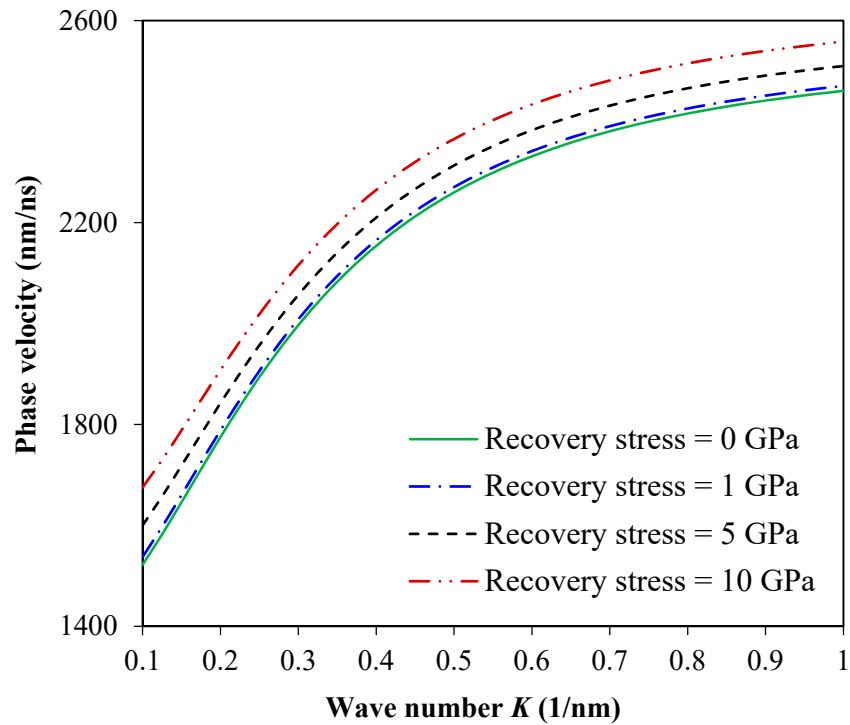


Figure 9. Effects of the recovery stress on the phase velocity of small-scale plates with SMA nanoscale wires.

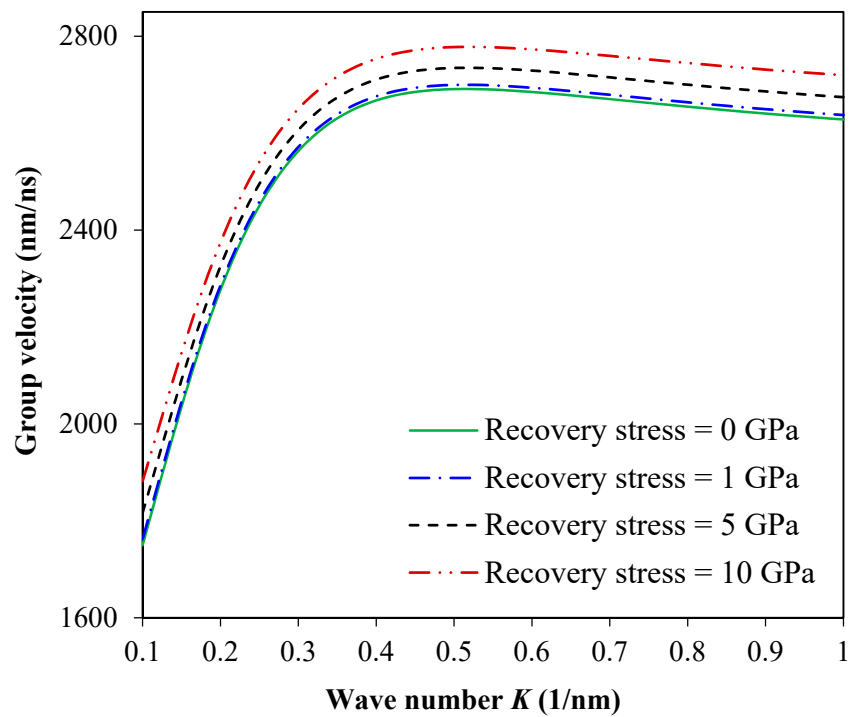


Figure 10. Effects of the recovery stress on the group velocity of small-scale plates with SMA nanoscale wires.

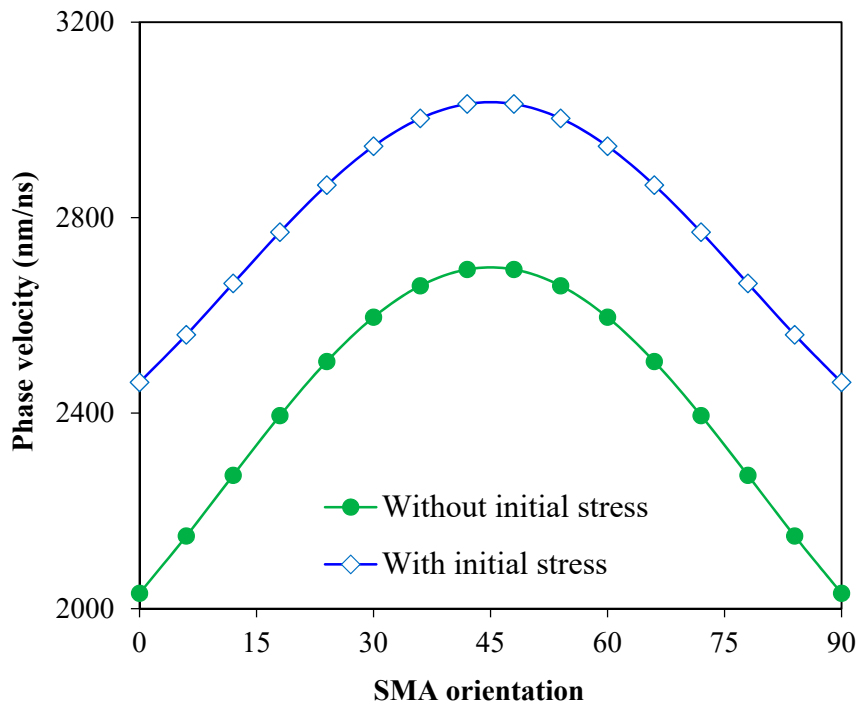


Figure 11. Effects of the wire orientation and initial stress on the phase velocity of small-scale plates with SMA nanoscale wires.

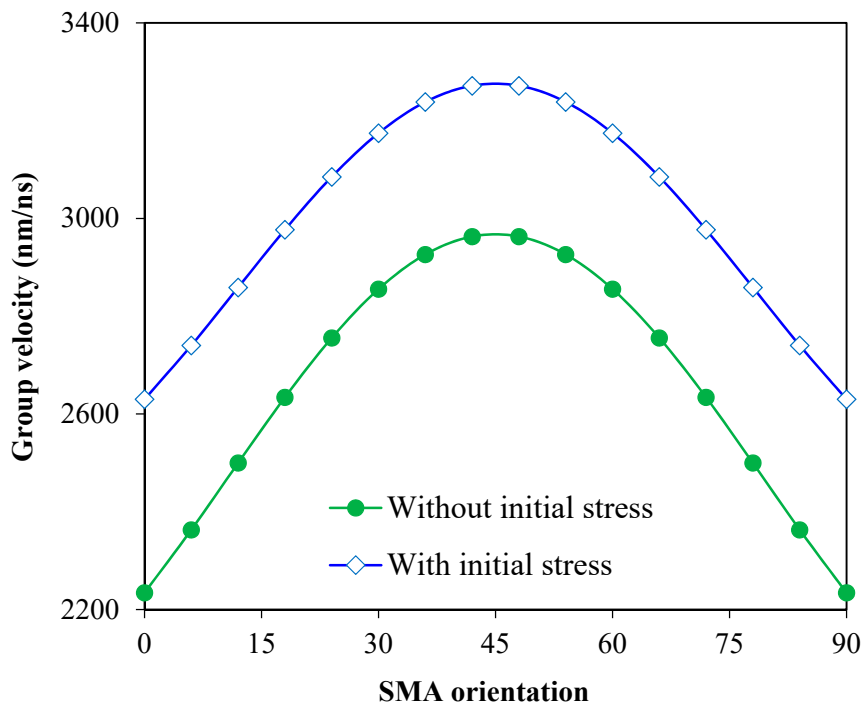


Figure 12. Effects of the wire orientation and initial stress on the group velocity of small-scale plates with SMA nanoscale wires.

Figures 13 and 14 are plotted in order to show the effects of a (i.e., the non-uniform coefficient) on the phase and group velocities of non-uniformly prestressed small-scale plates with SMA nanoscale wires, respectively. The initial stress ratio of the first layer, scale parameter and volume fraction are 0.5, 0.02 and 0.3, respectively. Moreover, the wave number is set to 1.0 1/nm. It is found that both phase and group velocities are highly dependent on the non-uniform coefficient. Greater values of this coefficient lead to greater phase and group velocities. Moreover, the various profiles of the biaxial

initial stress involving uniform, linear and quadratic are compared in Figures 15 and 16 for the phase and group velocities, respectively. The quadratic tensile profile leads to the greatest phase and group velocities whereas the uniform tensile profile results in the lowest phase and group velocities.

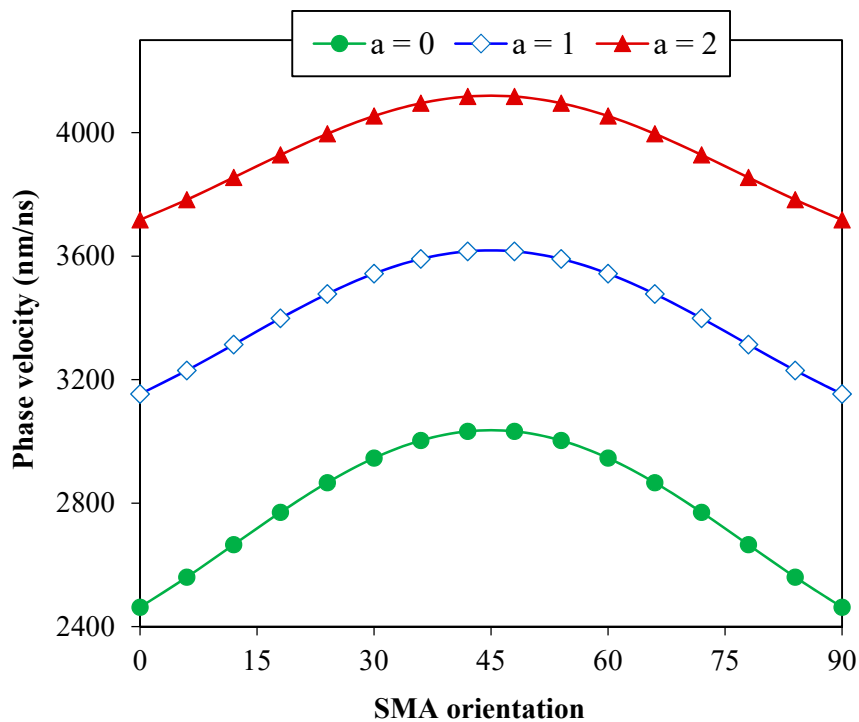


Figure 13. Effects of the non-uniform coefficient on the phase velocity of small-scale plates with SMA nanoscale wires.

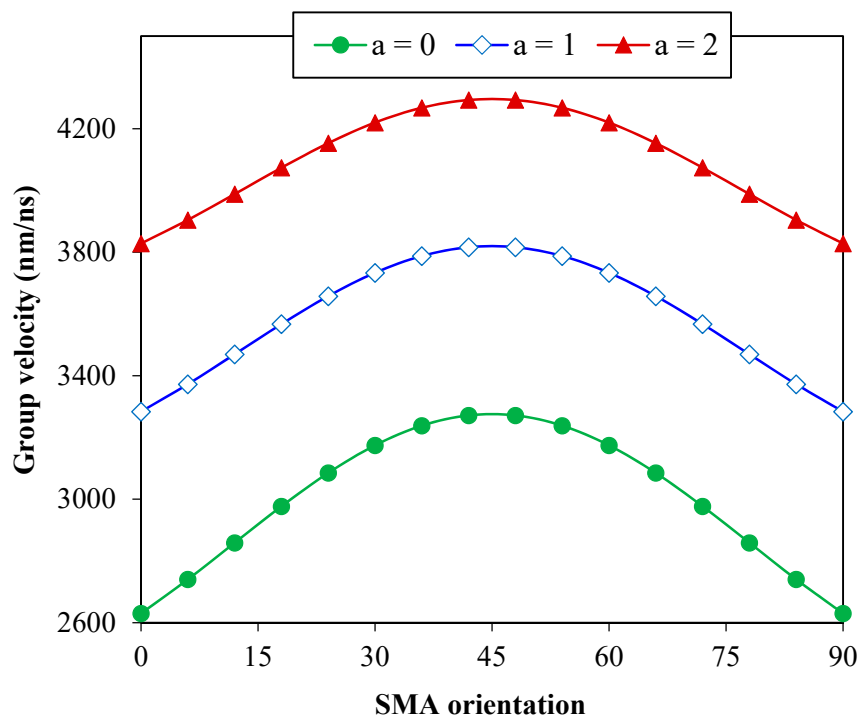


Figure 14. Effects of the non-uniform coefficient on the group velocity of small-scale plates with SMA nanoscale wires.

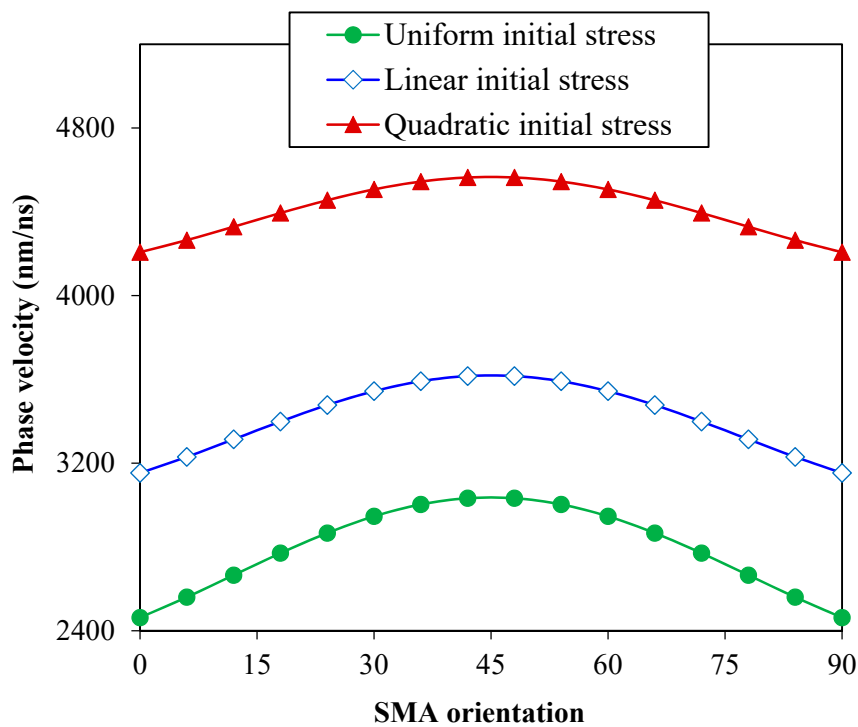


Figure 15. Effects of various profiles of initial stress on the phase velocity of small-scale plates with SMA nanoscale wires.

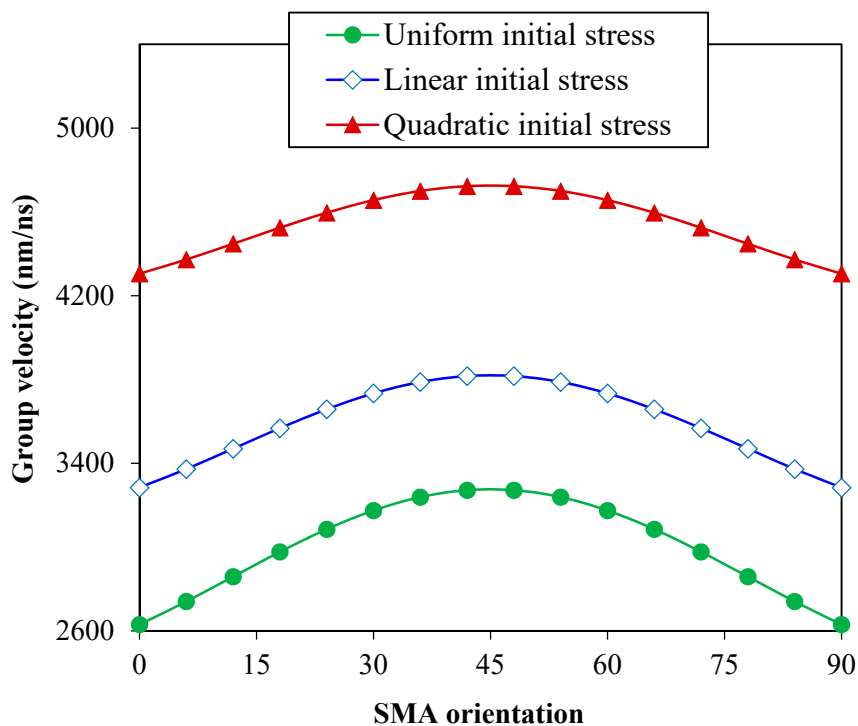


Figure 16. Effects of various profiles of initial stress on the group velocity of small-scale plates with SMA nanoscale wires.

4. Conclusions

The effects of non-uniformly distributed initial stresses on the wave propagation in small-scale plates with SMA nanoscale wires have been investigated. A scale-dependent model of plates was proposed utilizing the nonlocal elasticity in conjunction with Brinson’s model. The differential equations

for scale-dependent wave propagations in the small-scale system were derived. The influences of non-uniformly distributed initial stresses together with SMA effects on the phase and group velocities were explored. It was observed that a greater tensile initial stress leads to an increase in both the phase and group velocities of the small-scale plate with SMA nanoscale wires since tensile prestresses improve the total equivalent structural stiffness of reinforced multilayered small-scale plates. However, greater scale parameters of stress nonlocality result in lower phase and group velocities as this parameter has a decreasing influence on the equivalent structural stiffness. The volume fraction and orientation of SMA nanoscale wires can be utilized as a controlling factor for the wave propagation characteristics of prestressed small-scale plates. It was also found that both group and phase velocities increase when the non-uniform coefficient increases. The group and phase velocities of the small-scale plate with initial stress of quadratic tensile profile are higher than those of linear and uniform profiles.

Author Contributions: M.R.F.: Literature review, Mathematical modelling, Writing-original draft, Numerical analysis, Numerical solution. A.R.S.: Contribution to the conceptualization and modelling, Guidance, Writing-review and editing. A.F.: Contribution to the conceptualization and modelling, Guidance, Writing-review and editing. All authors have read and agreed to the published version of the manuscript.

Funding: This research received no external funding.

Conflicts of Interest: The authors declare no conflict of interest.

References

1. Rohani Rad, E.; Vahabi, H.; Formela, K.; Saeb, M.R.; Thomas, S. Injectable poloxamer/graphene oxide hydrogels with well-controlled mechanical and rheological properties. *Polym. Adv. Technol.* **2019**, *30*, 2250–2260. [[CrossRef](#)]
2. Vahabi, H.; Rad, E.R.; Parpaite, T.; Langlois, V.; Saeb, M.R. Biodegradable polyester thin films and coatings in the line of fire: The time of polyhydroxyalkanoate (PHA)? *Prog. Org. Coat.* **2019**, *133*, 85–89. [[CrossRef](#)]
3. Rad, E.R.; Vahabi, H.; de Anda, A.R.; Saeb, M.R.; Thomas, S. Bio-epoxy resins with inherent flame retardancy. *Prog. Org. Coat.* **2019**, *135*, 608–612. [[CrossRef](#)]
4. Rohani Rad, E.; Farajpour, M.R. Dynamics analysis of microparticles in inertial microfluidics for biomedical applications. *J. Comput. Appl. Mech.* **2019**, *50*, 157–164.
5. Goodarzi, M.; Mohammadi, M.; Farajpour, A.; Khooran, M. Investigation of the effect of pre-stressed on vibration frequency of rectangular nanoplate based on a visco-Pasternak foundation. *J. Solid Mech.* **2014**, *6*, 98–121.
6. Mohammadi, M.; Farajpour, A.; Goodarzi, M.; Dinari, F. Thermo-mechanical vibration analysis of annular and circular graphene sheet embedded in an elastic medium. *Lat. Am. J. Solids Struct.* **2014**, *11*, 659–682. [[CrossRef](#)]
7. Farajpour, M.R.; Shahidi, A.R.; Farajpour, A. Frequency behavior of ultrasmall sensors using vibrating SMA nanowire-reinforced sheets under a non-uniform biaxial preload. *Mater. Res. Express* **2019**, *6*, 065047. [[CrossRef](#)]
8. Malekzadeh, P.; Farajpour, A. Axisymmetric free and forced vibrations of initially stressed circular nanoplates embedded in an elastic medium. *Acta Mech.* **2012**, *223*, 2311–2330. [[CrossRef](#)]
9. Ebrahimejad, S.; Marzbanrad, J.; Boreiry, M.; Shaghghi, G.R. On the electro-thermo-mechanical vibration characteristics of elastically restrained functionally graded nanobeams using differential transformation method. *Appl. Phys. A* **2018**, *124*, 800. [[CrossRef](#)]
10. Ebrahimi, F.; Dabbagh, A. Effect of humid-thermal environment on wave dispersion characteristics of single-layered graphene sheets. *Appl. Phys. A* **2018**, *124*, 301. [[CrossRef](#)]
11. Arefi, M.; Zenkour, A.M. Vibration and bending analyses of magneto–electro–thermo-elastic sandwich microplates resting on viscoelastic foundation. *Appl. Phys. A* **2017**, *123*, 550. [[CrossRef](#)]
12. Xiao, W.; Li, L.; Wang, M. Propagation of in-plane wave in viscoelastic monolayer graphene via nonlocal strain gradient theory. *Appl. Phys. A* **2017**, *123*, 388. [[CrossRef](#)]
13. Jandaghian, A.; Rahmani, O. Buckling analysis of multi-layered graphene sheets based on a continuum mechanics model. *Appl. Phys. A* **2017**, *123*, 324. [[CrossRef](#)]

14. Ghadiri, M.; Hajbarati, H.; Safi, M. Vibration analysis of single-walled carbon peapods based on nonlocal Timoshenko beam theory. *Appl. Phys. A* **2017**, *123*, 260. [[CrossRef](#)]
15. Ansari, R.; Torabi, J. Numerical study on the free vibration of carbon nanocones resting on elastic foundation using nonlocal shell model. *Appl. Phys. A* **2016**, *122*, 1073. [[CrossRef](#)]
16. Kiani, K. Vibrations of fluid-conveying inclined single-walled carbon nanotubes acted upon by a longitudinal magnetic field. *Appl. Phys. A* **2016**, *122*, 1038. [[CrossRef](#)]
17. Farajpour, M.; Shahidi, A.; Farajpour, A. Elastic waves in fluid-conveying carbon nanotubes under magneto-hygro-mechanical loads via a two-phase local/nonlocal mixture model. *Mater. Res. Express* **2019**, *6*, 0850a8. [[CrossRef](#)]
18. Hadi, A.; Nejad, M.Z.; Hosseini, M. Vibrations of three-dimensionally graded nanobeams. *Int. J. Eng. Sci.* **2018**, *128*, 12–23. [[CrossRef](#)]
19. Nejad, M.Z.; Hadi, A. Non-local analysis of free vibration of bi-directional functionally graded Euler–Bernoulli nano-beams. *Int. J. Eng. Sci.* **2016**, *105*, 1–11. [[CrossRef](#)]
20. Aydogdu, M. Longitudinal wave propagation in multiwalled carbon nanotubes. *Compos. Struct.* **2014**, *107*, 578–584. [[CrossRef](#)]
21. Aydogdu, M. A nonlocal rod model for axial vibration of double-walled carbon nanotubes including axial van der Waals force effects. *J. Vib. Control* **2015**, *21*, 3132–3154. [[CrossRef](#)]
22. Malekzadeh, P.; Setoodeh, A.; Beni, A.A. Small scale effect on the thermal buckling of orthotropic arbitrary straight-sided quadrilateral nanoplates embedded in an elastic medium. *Compos. Struct.* **2011**, *93*, 2083–2089. [[CrossRef](#)]
23. Malekzadeh, P.; Shojaei, M. Surface and nonlocal effects on the nonlinear free vibration of non-uniform nanobeams. *Compos. Part B Eng.* **2013**, *52*, 84–92. [[CrossRef](#)]
24. Rohani Rad, E.; Farajpour, M.R. Influence of taxol and CNTs on the stability analysis of protein microtubules. *J. Comput. Appl. Mech.* **2019**, *50*, 140–147.
25. Wang, X.; Cai, H. Effects of initial stress on non-coaxial resonance of multi-wall carbon nanotubes. *Acta Mater.* **2006**, *54*, 2067–2074. [[CrossRef](#)]
26. Song, J.; Shen, J.; Li, X. Effects of initial axial stress on waves propagating in carbon nanotubes using a generalized nonlocal model. *Comput. Mater. Sci.* **2010**, *49*, 518–523. [[CrossRef](#)]
27. Heireche, H.; Tounsi, A.; Benzair, A.; Mechab, I. Sound wave propagation in single-walled carbon nanotubes with initial axial stress. *J. Appl. Phys.* **2008**, *104*, 014301. [[CrossRef](#)]
28. Güven, U. Transverse vibrations of single-walled carbon nanotubes with initial stress under magnetic field. *Compos. Struct.* **2014**, *114*, 92–98. [[CrossRef](#)]
29. Selim, M.; Abe, S.; Harigaya, K. Effects of initial compression stress on wave propagation in carbon nanotubes. *Eur. Phys. J. B* **2009**, *69*, 523–528. [[CrossRef](#)]
30. Shen, Z.-B.; Tang, G.-J.; Zhang, L.; Li, X.-F. Vibration of double-walled carbon nanotube based nanomechanical sensor with initial axial stress. *Comput. Mater. Sci.* **2012**, *58*, 51–58. [[CrossRef](#)]
31. Asemi, S.; Farajpour, A.; Asemi, H.; Mohammadi, M. Influence of initial stress on the vibration of double-piezoelectric-nanoplate systems with various boundary conditions using DQM. *Phys. E Low-Dimens. Syst. Nanostruct.* **2014**, *63*, 169–179. [[CrossRef](#)]
32. Wang, Y.-Z.; Li, F.-M.; Kishimoto, K. Scale effects on flexural wave propagation in nanoplate embedded in elastic matrix with initial stress. *Appl. Phys. A* **2010**, *99*, 907–911. [[CrossRef](#)]
33. Murmu, T.; Pradhan, S. Vibration analysis of nanoplates under uniaxial prestressed conditions via nonlocal elasticity. *J. Appl. Phys.* **2009**, *106*, 104301. [[CrossRef](#)]
34. Karami, B.; Shahsavari, D.; Janghorban, M.; Li, L. Wave dispersion of mounted graphene with initial stress. *Thin-Walled Struct.* **2018**, *122*, 102–111. [[CrossRef](#)]
35. Ebrahimi, F.; Shafiei, N. Influence of initial shear stress on the vibration behavior of single-layered graphene sheets embedded in an elastic medium based on Reddy’s higher-order shear deformation plate theory. *Mech. Adv. Mater. Struct.* **2017**, *24*, 761–772. [[CrossRef](#)]
36. Mohammadi, M.; Farajpour, A.; Goodarzi, M. Numerical study of the effect of shear in-plane load on the vibration analysis of graphene sheet embedded in an elastic medium. *Comput. Mater. Sci.* **2014**, *82*, 510–520. [[CrossRef](#)]

37. Phung-Van, P.; Lieu, Q.X.; Nguyen-Xuan, H.; Wahab, M.A. Size-dependent isogeometric analysis of functionally graded carbon nanotube-reinforced composite nanoplates. *Compos. Struct.* **2017**, *166*, 120–135. [[CrossRef](#)]
38. Kuang, Y.; Ou, J. Self-repairing performance of concrete beams strengthened using superelastic SMA wires in combination with adhesives released from hollow fibers. *Smart Mater. Struct.* **2008**, *17*, 025020. [[CrossRef](#)]
39. Ho, M.; McMillan, A.B.; Simard, J.M.; Gullapalli, R.; Desai, J.P. Toward a meso-scale SMA-actuated MRI-compatible neurosurgical robot. *IEEE Trans. Robot.* **2012**, *28*, 213–222. [[CrossRef](#)]
40. Kahn, H.; Huff, M.; Heuer, A. The TiNi shape-memory alloy and its applications for MEMS. *J. Micromech. Microeng.* **1998**, *8*, 213. [[CrossRef](#)]
41. Park, J.-S.; Kim, J.-H.; Moon, S.-H. Vibration of thermally post-buckled composite plates embedded with shape memory alloy fibers. *Compos. Struct.* **2004**, *63*, 179–188. [[CrossRef](#)]
42. Brinson, L.C. One-dimensional constitutive behavior of shape memory alloys: Thermomechanical derivation with non-constant material functions and redefined martensite internal variable. *J. Intell. Mater. Syst. Struct.* **1993**, *4*, 229–242. [[CrossRef](#)]
43. Farajpour, M.; Shahidi, A.; Farajpour, A. Influence of shear preload on wave propagation in small-scale plates with nanofibers. *Struct. Eng. Mech.* **2019**, *70*, 407–420.
44. Malekzadeh, P.; Shojaee, M. Free vibration of nanoplates based on a nonlocal two-variable refined plate theory. *Compos. Struct.* **2013**, *95*, 443–452. [[CrossRef](#)]
45. Asemi, S.R.; Farajpour, A.; Borghei, M.; Hassani, A.H. Thermal effects on the stability of circular graphene sheets via nonlocal continuum mechanics. *Lat. Am. J. Solids Struct.* **2014**, *11*, 704–724. [[CrossRef](#)]
46. Ebrahimi, F.; Barati, M.R.; Dabbagh, A. A nonlocal strain gradient theory for wave propagation analysis in temperature-dependent inhomogeneous nanoplates. *Int. J. Eng. Sci.* **2016**, *107*, 169–182. [[CrossRef](#)]
47. Allen, D.; Sayers, C. The measurement of residual stress in textured steel using an ultrasonic velocity combinations technique. *Ultrasonics* **1984**, *22*, 179–188. [[CrossRef](#)]
48. Vangi, D. Stress evaluation by pulse-echo ultrasonic longitudinal wave. *Exp. Mech.* **2001**, *41*, 277–281. [[CrossRef](#)]
49. Wang, Y.-Z.; Li, F.-M.; Kishimoto, K. Flexural wave propagation in double-layered nanoplates with small scale effects. *J. Appl. Phys.* **2010**, *108*, 064519. [[CrossRef](#)]
50. Farajpour, M.; Shahidi, A.; Farajpour, A. A nonlocal continuum model for the biaxial buckling analysis of composite nanoplates with shape memory alloy nanowires. *Mater. Res. Express* **2018**, *5*, 035026. [[CrossRef](#)]

